**Solid Freeform Fabrication 2021: Proceedings of the 32nd Annual International Solid Freeform Fabrication Symposium – An Additive Manufacturing Conference**
**Reviewed Paper**

# Effect of Voronoi Lattice Geometry on the Fatigue Performance of Ti-6Al-4V

S.M. Uí Mhurchadha[1], S. Marques[1], L. Givet[1], R. Raghavendra[1, 2]

[1] SEAM Research Centre, School of Engineering, Waterford Institute of Technology, Ireland
[2] I-Form Advanced Manufacturing Research Centre, Ireland

## Abstract

This paper investigates the effect of strut thickness and number of pores on the fatigue performance of Ti-6Al-4V voronoi lattice structures designed with the same part volume. The aim of this study is to establish the variation in high cycle fatigue parameters for constant volume lattice structures designed with various lattice parameters. Voronoi geometries were designed with varying strut thicknesses and number of pores to maintain a constant specimen volume. The geometries were tested under compressive fatigue conditions at a reversal ratio, R, of 0.1. It was found that the strut thickness has a significant influence on the fatigue life of the lattice. An increase in the strut thickness by 100 μm can result in a reduction in fatigue life by up to a factor of 10. The results from this research can influence the design of lattice structures for osteointegration in load-bearing biomedical implant applications.

***Keywords:*** High-cycle fatigue, Metamaterials, Laser Powder Bed Fusion, Fatigue life

## Introduction

Additive manufacturing (AM) allows for the manufacture of complex lattice structures by using a layer-by-layer approach to manufacturing parts. Lattice structures are also known as metamaterials, which are structures that are designed so that their properties are primarily geometrically-driven. For biomedical applications, these lattice structures can be used in orthopaedic implants to promote osseointegration, as well as mimicking the mechanical properties of human bone. Typically, for orthopaedic implants, the pore size range of these lattice structures should be in the range of 150 to 600 μm [1]. The reported porosity of trabecular bone ranges from 50 to 90 % [2, 3]. Biocompatible materials, such as the Titanium alloy, Ti-6Al-4V, are used for the manufacture of orthopaedic implants.

Researchers have used various methods of generating bio-mimicking lattice structures, such as repeated cellular units [4, 5], TPMS (triply periodic minimal surface) [6, 7], stochastic lattices based on a Poisson disk algorithm [4, 8, 9] and Voronoi tessellation [10, 11]. This research focuses on the Voronoi tessellation method. A Voronoi lattice is a 3D isotropic porous interconnected model that can be designed to mimic the physical properties of bone, such as trabecular thickness, trabecular separation, trabecular number, bone volume to total volume ratio and bone surface to bone volume ratio, for example [11].

Load-bearing implants in the body undergo cyclic compressive loading, which can result in fatigue damage in extreme cases. ASTM [12] defines fatigue as "the progressive, localised permanent structural change occurring in a material subjected to conditions which produce fluctuating stresses and strains at some point or points which may culminate as cracks". Under fatigue loading, failure of materials can be observed at loads less than the monotonic yield strength of the material. Fatigue can be categorised into either high-cycle fatigue (HCF) or low-cycle fatigue (LCF), depending on the number of cycles to failure, $N_f$. The total life, $N_f$, is represented as the sum of the number of cycles to crack initiation, $N_i$, and the number of cycles for the crack to propagate to a detectable or critical length, $N_P$, where $N_f = N_i + N_P$. Wöhler [13, 14] was the first to carry out a systematic study on fatigue. A relationship between stress and fatigue life was observed; the stress range has a greater influence on fatigue life than the peak stress [15]. From this work, S-N (stress vs number of cycles to failure) curves were proposed to estimate fatigue lives; this S-N curve method is still used today. Since then, many researchers have developed fatigue failure criterion based on stress [16, 17, 18] or strain [19, 20] conditions.

Recently, researchers have investigated the fatigue behaviour of metallic metal-biomaterials. The primary loading conditions on orthopaedic implants are compression and bending. Therefore, many researchers, e.g. [21, 22, 23, 24, 25, 26], have investigated the compressive fatigue loading of bone-mimicking bio-metamaterials, establishing S-N curves for the metamaterials.

This paper investigates the effect of the geometry lattice parameters on the fatigue behaviour of Ti-6Al-4V Voronoi lattices manufactured via Laser Powder Bed Fusion (L-PBF). To this end, lattice structures are

designed to have the same volume, i.e. the same lattice density, but different lattice parameters, such as strut thickness and number of pores. Two lattice geometries are designed with strut thickness differing by 100 µm. These lattices are then tested in compressive fatigue under high cycle fatigue loading conditions. S-N curves are derived from the experimental results and high-cycle fatigue parameters calculated.

## Methodology

### Design and manufacture of lattice specimen

Voronoi lattice structures were designed using nTopology software [27]. The test samples were designed based on ISO 13314 [28] standard for the compression testing of porous and cellular metals. Cylindrical specimen of diameter 10 mm and height of 15 mm [28] were used for the two lattice geometries, presented in Figure 1, were designed and used in this study. The density of the lattices was design to be approximately 20 %. Often the density of a porous structure is predefined, for example to match the density of a particular bone type. Therefore, for this study a constant density was used for the design to investigate the effect of the geometry variables that result in the same density. The design parameters for the two geometries are presented in Figure 1.

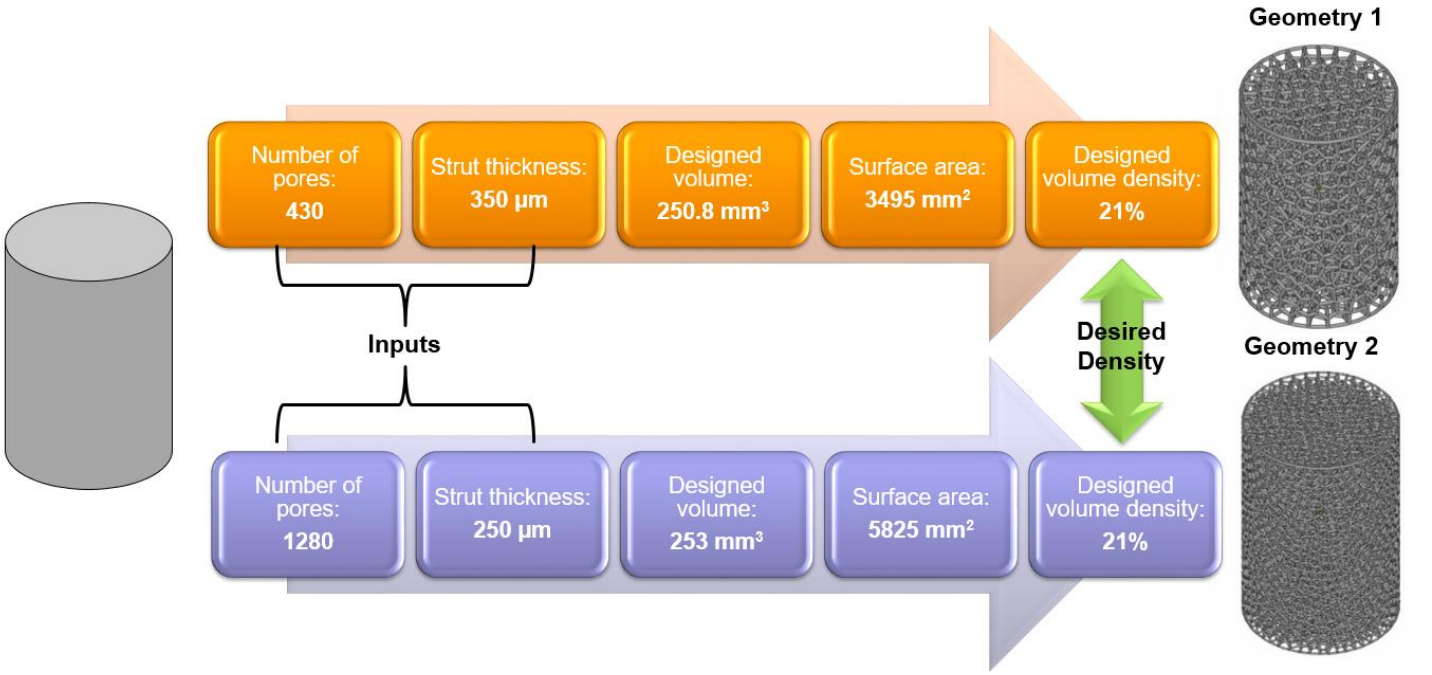


Figure 1. Two Voronoi lattice geometries used in this study, Geometry 1 and Geometry 2, with the same part density, but different strut thicknesses and number of pores.

Ten of each lattice structure presented in Figure 1 were manufactured via L-PBF on an EOS M100 machine. The material used was Grade 23 Ti-6Al-4V ELI (Extra Low Interstitials) supplied by Carpenter Additive [29]. The laser spot size of the EOS M100 machine was approximately 40 µm. The build chamber was maintained at 40 ºC and under an inert Argon atmosphere throughout the manufacturing process. The specimen were removed from the build plate using Wire EDM. Powder was removed for the lattice structures using a combination of dry ice blasting and ultrasonic cleaning.

### Characterisation of lattices

The volume of the manufactured lattices was measured using Helium gas pycnometry on a Micrometics Accupyc 1340 gas pycnometer. This is a volume measurement methodology based on Boyle's Law. The specimen is placed in a chamber and Helium (He) is pumped into the chamber to a known a set pressure. This volume of He is then released into a second chamber of known volume and the pressure of the gas in this chamber is measured. From this, the volume of the lattice structure is calculated. The pycnometry tests were repeated five times per sample and then averaged. He gas was used as it has low density and can penetrate small surface pores to get an accurate measurement of the volume. The mass of each specimen was also measured.

**Fatigue testing**

Compressive fatigue tests were conducted on the specimen using an Instron Electropulse 3 kN testing machine at a frequency of 15 Hz [22]. A reversal load ratio, $R$, of 0.1 was used for the loading conditions, ensuring that the specimen were under compressive loading throughout all tests. $R$ is given by:

$$R = \frac{F_{min}}{F_{max}} \tag{1}$$

where $F_{\min}$ and $F_{\max}$ are the minimum and maximum forces for each fatigue cycle. The maximum and minimum applied forces for each loading condition is presented in Table. The fatigue tests were stopped after 1 million cycles if the specimen did not fail.

Table 1. Loading conditions for compressive fatigue testing of lattices.

| Loading Condition | $F_{\max}$ (N) | $F_{\min}$ (N) |
|---|---|---|
| **LC1** | -2852 | -285.2 |
| **LC2** | -2333 | -233.3 |
| **LC3** | -1815 | -181.5 |
| **LC4** | -1296 | -129.6 |
| **LC5** | -778 | -78.8 |

**Fatigue material model**

From the fatigue test results, S-N curves for each lattice geometry were correlated. The stress was calculated based on the force per unit area, which was calculated based on the average cross-sectional area per unit height of the lattice. A comparison between the designed geometry and actual geometry was investigated.

Basquin [17] developed the stress-life approach, by observing a log-log relationship between stress amplitude and the fatigue life for high-cycle fatigue (HCF). The Basquin equation is given by:

$$\frac{\Delta\sigma}{2} = \sigma_f'\left(2N_f\right)^b \tag{2}$$

where $\Delta\sigma$ is the stress range, $\sigma_f'$ is the fatigue strength coefficient and b is the fatigue strength exponent. Fatigue parameters for the two lattice geometries are compared.

## Results and discussion

**Characterisation of manufactured lattices**

The measured volumes for the two lattice geometries are presented in Figure 2. There is a large difference between the designed and manufactured volumes. This is associated with the partially sintered particles on the struts of the lattice, as well as the surface roughness of these struts. This has a larger effect of the lattice volume for Geometry 2, due to the larger surface area associated with the thinner struts combined with the larger number of pores. The strut thicknesses of the two geometries are shown in the SEM images presented in Figure 3. The average strut thickness of the as-build Geometry 1 is 350 µm, which is the same as the designed strut thickness. However, the average strut thickness for Geometry 2 is 290 µm, which is 40 µm larger than the designed thickness. This can be attributed to the accuracy of the laser in the L-PBF for hatch strategies for smaller parts.

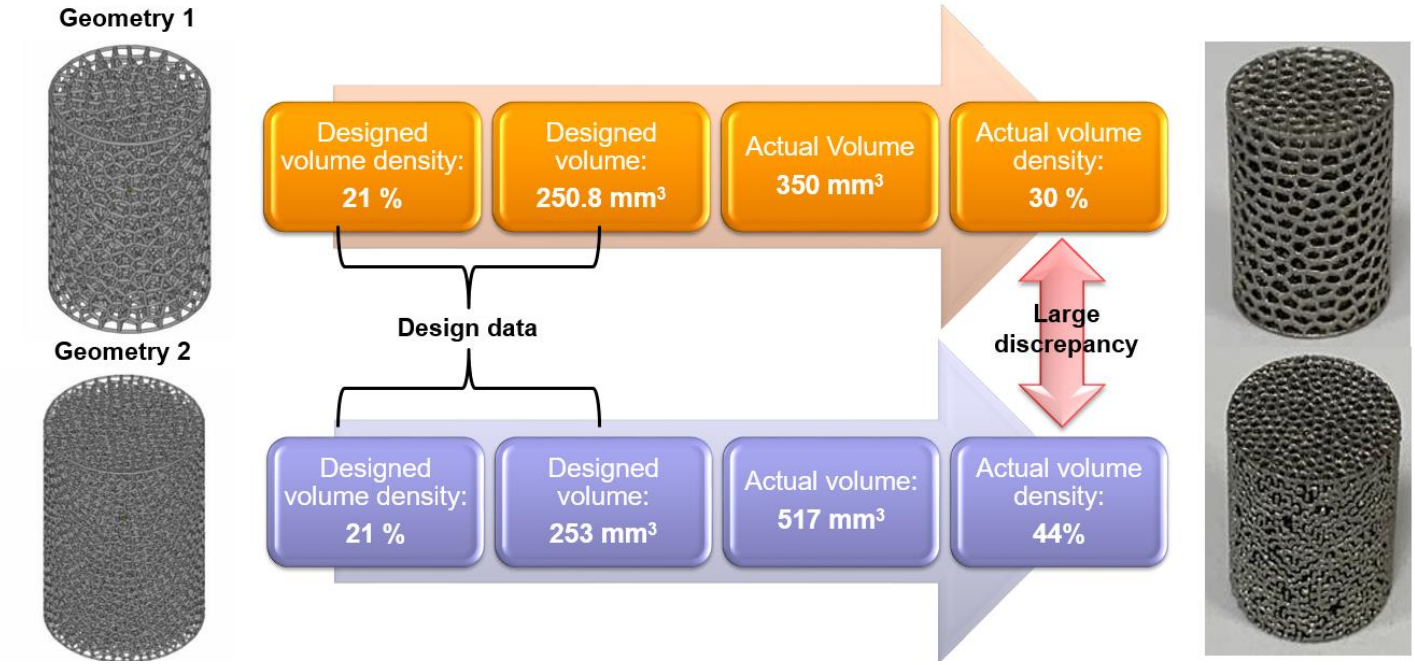


Figure 2. Manufactured volumes and densities of the two voronoi geometries compared to the design criteria.

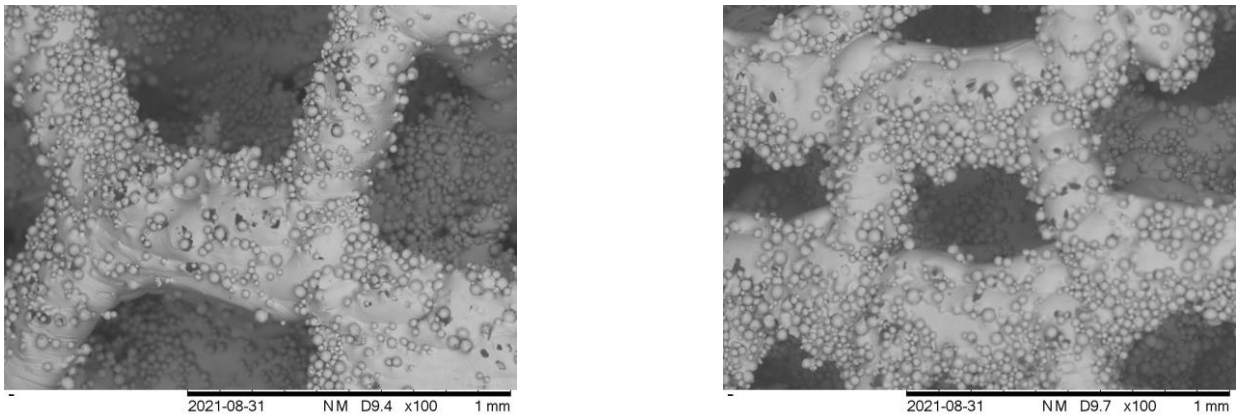


(a) (b)

Figure 3. SEM images of (a) Geometry 1 with an average strut thickness of 350 µm, and (b) Geometry 2 with average strut thickness of 290 µm.

**Fatigue life of lattices**

Figure  presents the force-displacement loading loops for both geometries, for the maximum loading conditions, i.e. $F_{max}$ of 2.852 kN, at for initial cycle, mid-cycle and final cycle of the compressive fatigue test. These loops confirm that no plasticity occurred in the samples during testing and therefore, all fatigue tests conducted were under high cycle fatigue loading conditions. However, it is possible that some localised plasticity occurred at highly localised stress concentrations within the lattice structure. Therefore, Figure  demonstrates that the dynamic mechanical behaviour of the metamaterial was elastic and therefore, tested in high cycle fatigue.

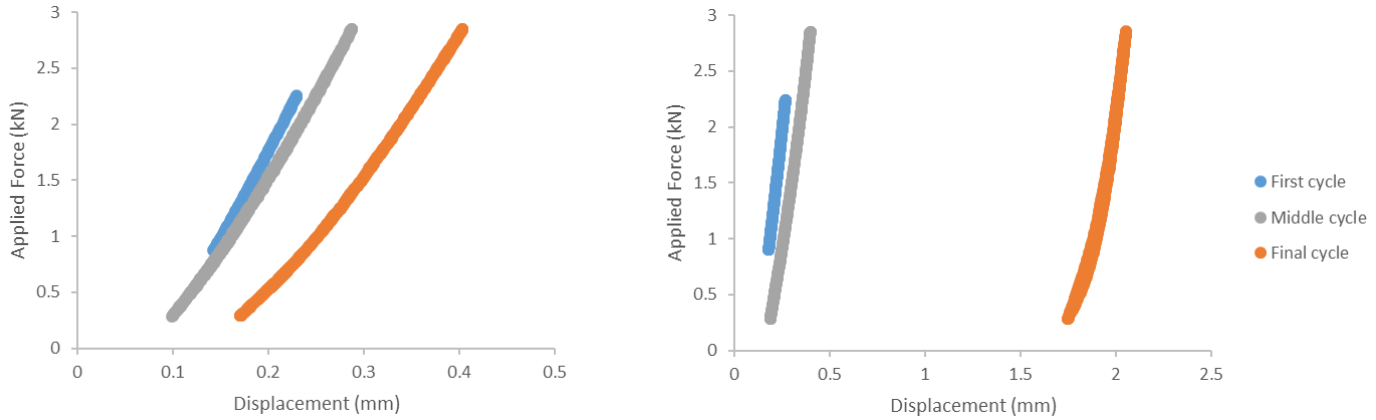


(a) (b)

Figure 4. Force displacement loops for the initial cycle, a mid-cycle and the final cycle for LC1 compressive fatigue loading conditions on (a) Geometry 1, and (b) Geometry 2.

Summaries of the minimum and maximum stresses for each loading condition on the two geometries are presented in Figure . The stresses presented here are based on the designed cross-sectional area of the specimen. This is to highlight the requirement to determine the actual cross-sectional area of the lattices after manufacturing. For Geometry 1 (Figure (a)), the test reached 1 million cycles for LC3, as presented in Table. Whereas, Geometry 2 (Figure (b)) reached 1 million cycles for LC5 as presented in Table. For both geometries, a life of over $10^6$ cycles was determined to be infinite cycles. A considerable difference can be seen between the two geometries.

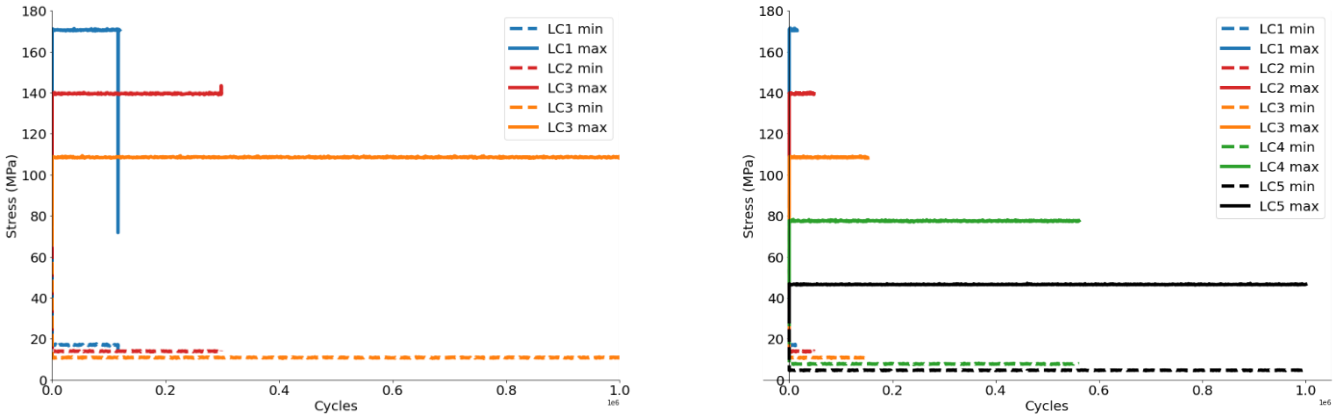


(a) (b)

Figure 5. Minimum and maximum stress evolution, as calculated using the designed cross-sectional area, for each load case, as presented in Table, for (a) Geometry 1, and (b) Geometry 2.

Figure presents the evolutions of the minimum and maximum actual stresses, based on the measured L-PBF lattices, for each loading condition on the two geometries. As expected from the measured volume results presented in Figure 2, the actual stresses are lower compared to those presented in Figure 5. Geometry 2 has a significantly lower load-bearing capacity compared to Geometry 1. For Geometry 2, LC2 had a maximum compressive stress range ($\Delta\sigma/2 = (|\sigma_{max} - \sigma_{min}|)/2$) of 33 MPa, similar to the compressive range stress of 39 MPa experienced by Geometry 1 for LC3. However, Geometry 1 test was considered to run infinitely i.e. greater than $10^6$ cycles, whereas, Geometry 2 failed after $4.8 \times 10^4$ cycles. This is a considerable difference in the dynamic load-bearing capability of the two structures under similar loading conditions. Despite Geometry 2 being manufactured to have a larger cross-sectional area, it has a lower fatigue load carrying capabilities compared to Geometry 1. This can be attributed to the increased surface area of Geometry 2, which provides more crack initiation points, combined with the thinner struts, meaning that once a crack initiations, it requires fewer cycles to propagate to failure of the structure.

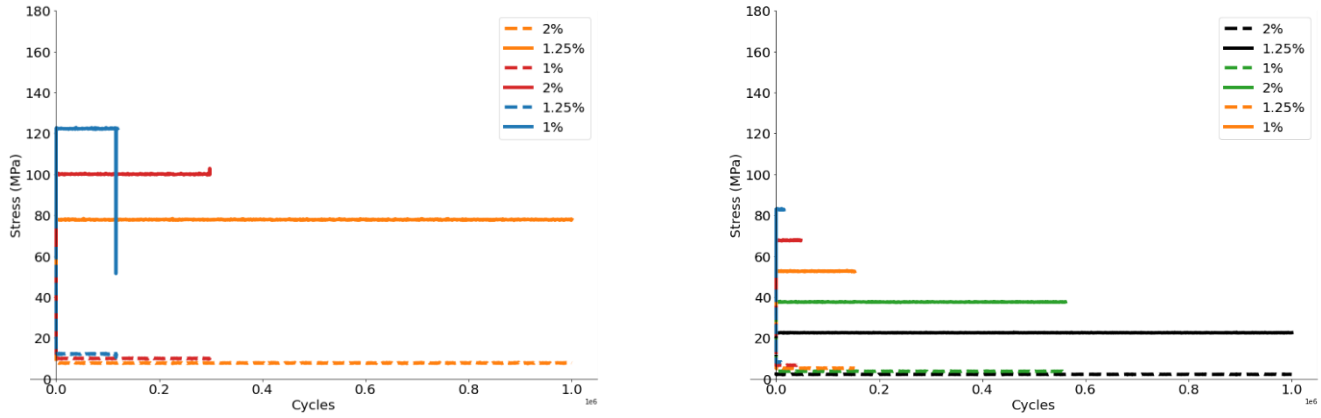


(a) (b)

Figure 6. Minimum and maximum stress evolution, as calculated using the actual cross-sectional area, for each load case, as presented in Table, for (a) Geometry 1, and (b) Geometry 2.

Figure 7 presents the S-N curves for Geometry 1 and Geometry 2, as calculated for the design stress (Figure 7 (a)) and the actual stress (Figure (b)) for each sample. For both the design and the actual stress graphs, a significant difference between the two geometries can be observed. As seen in Figures 5 and 5, Geometry 1 have a greater dynamic load-bearing capacity compared to Geometry 2. Critically, there is a significant difference between the S-N curves, as calculated using the designed cross-sectional area and as calculated using the actual cross-sectional area. For example, for Geometry 2 and at a stress range of 40 MPa, the fatigue life using the actual cross-sectional area S-N curve is in the range of $1.5 \times 10^4$; whereas, if the designed cross-sectional area S-N curve is used, the fatigue life is in the range of $5.6 \times 10^5$. This represents a factor greater than 10 between the two S-N curves, highlighting the requirements to measure the actual manufactured lattice structure rather relying solely on the design data.

Overall, Geometry 2 has a considerably lower fatigue life, compared to Geometry 1. This can be attributed to a few different factors. Firstly, the thinner struts in Geometry 2 results in fewer microstructural grains in the cross-section of the strut, compared to Geometry 1. Grain boundaries have been shown to hinder crack propagation of fatigue cracks, resulting in increased cycles for crack propagation [30]. Therefore, the greater the number of grain boundaries in a cross-section of a lattice strut, the greater the number of cycles for crack propagation. Furthermore, the larger number of pores in the lattice of Geometry 2 means that there is a larger probability of a stress concentration occurring. These stress concentration also have a larger effect on the structure of Geometry 2 due to the thinner struts. Finally, as presented in Figures 2 and 3, Geometry 2 has a larger surface area compared to Geometry 1. This provides more area for crack initiation points, which are further exacerbated by the inherent surface roughness from L-PBF.

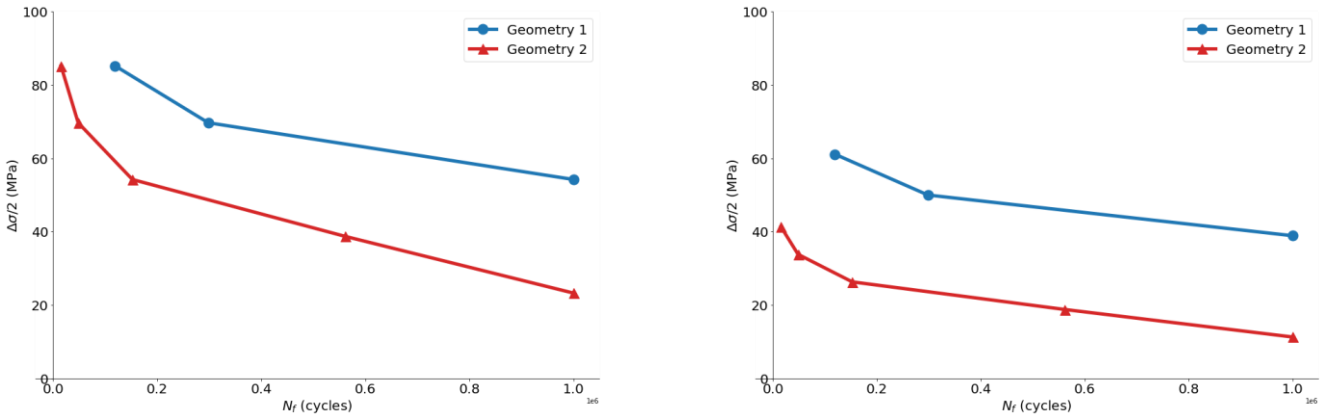


(a) (b)

Figure 7. S-N curves for Geometry 1 and Geometry 2 for (a) the design stress for each sample, and (b) the actual stress for each samples.

**Fatigue coefficients**

Basquin parameters ($\sigma_f'$ and b) can be estimated from monotonic test data using the universal slopes method [17, 31]. This method gives estimated fatigue coefficients based on monotonic tensile test results for ultimate tensile strength, $\sigma_{UTS}$, e.g. $\sigma_f' = 1.9\sigma_{UTS}$, and b = −0.12. This method has been used to provide a baseline for the high-cycle fatigue parameters for L-PBF Ti-6Al-4V, presented in Table 2 [30].

Basquin high-cycle fatigue parameters for Geometries 1 and 2 were obtained from the HCF test data presented above. Table 2 also presents the Basquin high-cycle fatigue parameters for Geometries 1 and 2, based on the stress calculated using the designed cross-sectional area. The fatigue strength exponent, $b$, is about twice that of the baseline for L-PBF Ti-6Al-4V, shown in Table 2. The fatigue strength coefficients, $\sigma_f'$, for both geometries are lower than that of the baseline for L-PBF Ti-6Al-4V. The Basquin high-cycle fatigue parameters for Geometries 1 and 2, based on the stress calculated using the actual cross-sectional area of the parts are also presented. The fatigue strength exponent, b, for each geometry is the same as those presented in Table 2. However, the fatigue strength coefficients, $\sigma_f'$, for both geometries are lower than those calculated for the designed cross-sectional area of the specimen.

Table 2. Baseline high-cycle fatigue parameters for L-PBF Ti-6Al-4V, calculated using the Universal Slopes Method [31] and for Geometries 1 and 2, calculated using the designed and manufactured cross-sectional areas of the structures.

| | Material | $\sigma_f'$ (MPa) | $b$ |
|---|---|---|---|
| **Universal slopes method [30]** | **Ti-6Al-4V** | 1710 | -0.12 |
| **Based on designed geometry** | **Geometry 1** | 1360 | -0.21 |
| | **Geometry 2** | 908 | -0.22 |
| **Based on manufactured geometry** | **Geometry 1** | 975 | -0.21 |
| | **Geometry 2** | 470 | -0.22 |

Figure  presents HCF experimental test results with Basquin fit for Geometries 1 and 2, from Table 2, compared to the baseline Basquin equation for L-PBF Ti-6Al-4V, for the stress range calculated using the designed cross-sectional areas (Figure  (a)) and the actual cross-sectional areas for the specimen (Figure  (b)). There is a good fit between the experimental data and the Basquin equations.

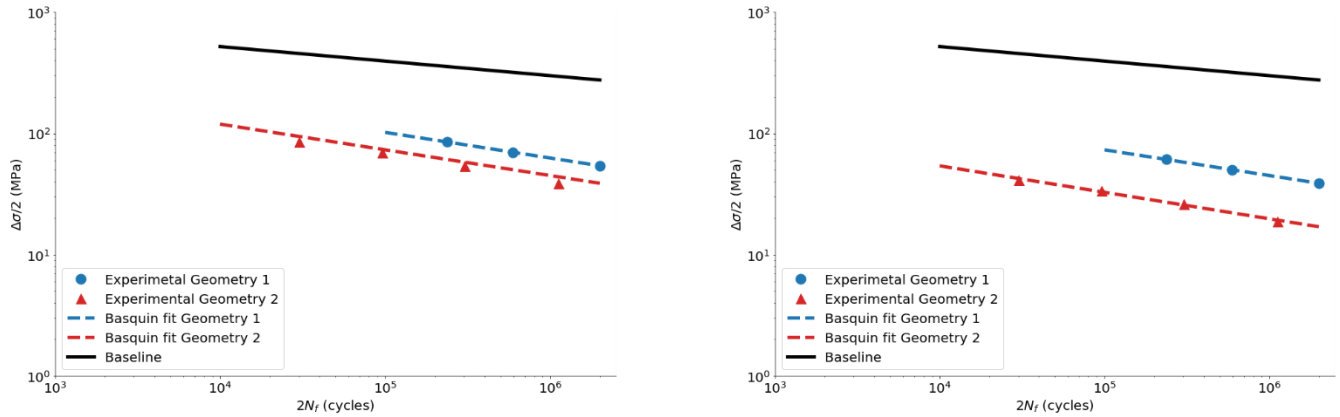


(a) (b)

Figure 8. HCF experimental test results with Basquin fit for Geometries 1 and 2, compared to the baseline Basquin equation for L-PBF Ti-6Al-4V, for the stress range calculated using (a) the designed cross-sectional areas, and (b) the actual cross-sectional areas for the specimen.

**Discussion**

The use of the Basquin equation alone assumes that the fatigue loading on the structures is uniaxial, where the largest principal stress is much greater than the other principal stresses. Due to the design of the structures, a

multiaxial fatigue approach may be more accurate for the prediction of fatigue in complex structures. In lattice structures, multiaxial fatigue can be further complicated by the potential for non-proportional loading. Under proportional loading conditions the principal stresses remain in constant proportion to each other, and hence the angle of the principal axes remains constant throughout the fatigue cycle. Non-proportional or out-of-phase loading results in extra cyclic hardening due to the rotation of principal axes. The critical plane approach was developed from the work of Brown and Miller [32]. It is based on the physical observation that fatigue cracks initiate and grow on certain planes within a material, where the crack growth and orientation depend on the normal stresses and/or shear stresses and strains on these planes [33]. The planes on which most fatigue damage occurs are called critical planes. This approach overcame the limitations of the Brown and Miller [32] approach with respect to the increased damage associated with out-of-plane loading.

## Conclusions

This paper presented an investigation into the effect of Voronoi lattice geometry on the fatigue performance of Ti-6Al-4V. Two different lattice structures with the same overall lattice density were design in nTopology. The strut thicknesses of the lattices differed by 100 μm. Therefore, the number of pores also different, to maintain a constant volume between the designs. These designs were manufactured via L-PBF and the differences between the designed and manufactured part correlated. The two lattice geometries were dynamically tested under compressive fatigue loading and fatigue parameters defined. The primary findings of the paper can be concluded as follows:

- A lattice geometry design with a larger surface area results in a larger discrepancy between the designed volume and the actual L-PBF manufactured volume. This is due to the adherence of particles to the surface of the lattice struts. The increased surface area resulted in more crack initiation points due to the inherent surface roughness of L-PBF parts.
- The high-cycle fatigue load-bearing capacity of the lattices structure is highly dependent on the lattice geometry, in particular, the strut thickness. The lattice structure with thinner struts exhibited considerably lower fatigue strength compared to the thicker lattice with larger strut thickness.
- A reduction in lattice strut thickness can result in a reduction in the fatigue life of the lattice by a factor of 10.
- It is essential to measure the difference between the designed and actual cross-sectional area of the lattice structures. Failure to do so could result in the over prediction of fatigue life of a component.

Finally, this paper has outlined the high cycle fatigue performance considering the lattices structure as a metamaterial. However, further in depth studies of the multi-axial fatigue of a lattice structure will provide an understanding into the failure mechanisms. This will require the implementation of critical plane multi-axial fatigue analysis of lattices structures under dynamic loading within a finite element simulation. By understanding the failure mechanisms of the lattice structures, the design of lattices can be tuned to prolong the fatigue life of the structures.

## Acknowledgements

The authors wish to acknowledge 3DWIT for the Wire EDM of the samples from the build plate.

## References

[1] C. Cornell, “Osteoconductive materials and their role as substitutes for autogenous bone grafts,” *Orthopedic Clinics of North America,* vol. 30, no. 4, pp. 591-598, 1999.

[2] S. Hollister and M. Kikuchi, “Homogenization theory and digital imaging: a basis for studying the mechanics and design principles of bone tissue,” *Biotechnology and Bioengineering,* vol. 43, no. 7, pp. 586-596, 1994.

[3] A. Salgado, O. Coutinho and R. Reis, “Bone tissue engineering: state of the art and future trends,” *Macromolecular Bioscience,* vol. 4, no. 8, pp. 743-765, 2004.

[4] M. Munford, U. Hossain, S. Ghouse and J. Jeffers, “Prediction of anisotropic mechanical properties for lattice structures,” *Additive Manufacturing,* vol. 32, 2020.

[5] S. Ahmadi, R. Hedayati, Y. Li, K. Lietaert, N. Tümer, A. Fatemi, C. Rans, B. Pouran, H. Weinans and A. Zadpoor, "Fatigue performance of additively manufactured meta-biomaterials: The effects of topology and material type," *Acta Biomaterialia,* vol. 65, pp. 292-304, 2018.

[6] F. Bobbert, K. Lietart, A. Eftekhari, B. Pouran, S. Ahmadi, H. Weinans and A. Zadpoor, "Additively manufactured metallic porous biomaterials based on minimal surfaces: A unique combination of topological, mechanical, and mass transport properties," *Acta Biomaterialia,* vol. 53, pp. 572-584, 2017.

[7] M. Afshar, A. Pourkamali Anarki, H. Montazerian and J. Kadkhodapour, "Additive manufacturing and mechanical characterization of graded porosity scaffolds designed based on triply periodic minimal surface architectures," *Journal of the Mechanical Behavior of Biomedical Materials,* vol. 62, pp. 481-494, 2016.

[8] S. Ghouse, S. Babu, K. Nai, P. Hooper and J. Jeffers, "The influence of laser parameters, scanning strategies and material on the fatigue strength of a stochastic porous structure," *Additive Manufacturing,* vol. 22, pp. 290-301, 2018.

[9] S. Ghouse, S. Babu, R. Van Arkel, K. Nai, P. Hooper and J. Jeffers, "The influence of laser parameters and scanning strategies on the mechanical properties of a stochastic porous material," *Materials and Design,* vol. 131, pp. 498-508, 2017.

[10] M. Fantini, M. Curto and F. De Crescenzio, "A method to design biomimetic scaffolds for bone tissue engineering based on Voronoi lattices," *Virtual and Phyciscal Prototyping,* vol. 11, no. 2, pp. 77-90, 2016.

[11] S. Gómez, M. Vlad, J. López and E. Fernández, "Design and Properties of 3D Scaffolds for Bone Tissue Engineering," *Acta Biomaterialia,* vol. 42, pp. 341-350, 2016.

[12] ASTM, *Standard terminology relating to fatigue and fracture testing,* ASTM International, 2014.

[13] A. Wöhler, "Bericht über die Versuche, welche auf der Königl. Niederschlesisch-Märkischen Eisenbahn mit Apparaten zum Messender Biegung und Verdrehung von Eisen bahnwagenachsen während der Fahrt angestellt wurden.," *Z. Bauwes. Bd,* 1858.

[14] A. Wohler, "Versuche zur ermittlung der auf die eisenbahnwagenachsen einwirkenden krafte und die widerstandsfahigkeit der wagen-achsen.," *Zeitschrift für Bauwes,* p. 583–616, 1860.

[15] A. Wöhler, "Über die Festigkeitsversuche mit Eisen und Stahl. Auf Anordnung des Ministers für Handel, Gewerbe u. öffentl," *Arbeiten, Grafen Itzenblitz, angestellt. Ernst und Korn, Berlin.,* 1870.

[16] J. Goodman, 1899, London : Longmans Green, Mechanics applied to engineering.

[17] O. Basquin, "The exponential law of endurance tests," *Proceedings of the American Society for Testing and Materials,* pp. 625-630, 1910.

[18] C. Soderberg and V. Sweden, "Factor of safety and working stress," *Transcripts of American Society for Testing of Materials,* vol. 52, pp. 13-28, 1930.

[19] L. Coffin, "A study of the effects of cyclic thermal stress on a ductile metal," *Transcripts of the Americian Society of Mechanical Engineering,* vol. 76, pp. 931-950, 1954.

[20] S. Manson, "Fatigue: A Complex Subject-Some Simple Approximations," *Experimental Mechanics ,* vol. 5, no. 4, pp. 193-226, 1965.

[21] S. Amin Yavari, S. Ahmadi, R. Wauthle, B. Pouran, J. Schrooten, H. Weinans and A. Zadpoor, "Relationship between unit cell type and porosity and the fatigue behavior of selective laser melted meta-biomaterials," *Journal of the Mechanical Behavior of Biomedical Materials,* vol. 43, pp. 91-100, 2015.

[22] N. Hrabe, P. Heinl, B. Flinn, C. Körner and R. Bordia, "Compression-compression fatigue of selective electron beam melted cellular titanium (Ti-6Al-4V)," *Journal of Biomedical Materials Research Part B,* vol. 99, no. 2, pp. 313-320, 2011.

[23] S. Zhao, S. Li, W. Hou, Y. Hao, R. Yang and R. Misra, "The influence of cell morphology on the compressive fatigue behavior of Ti-6Al-4V meshes fabricated by electron beam melting," *Journal of the Mechanical Behavor of Biomedical Materials,* vol. 59, pp. 251-264, 2016.

[24] G. Yan, L. Hao, A. Hussein and P. Young, “Ti–6Al–4V triply periodic minimal surface structures for bone implants fabricated via selective laser melting,” *Journal of the Mechanical Behavior of Biomedical Materials,* vol. 51, pp. 61-73, 2015.

[25] S. Yavari, S. Ahmadi, R. Wauthle, B. Pouran, J. Schrooten, H. Weinans and Zadpoor, “Relationship between unit cell type and porosity and the fatigue behavior of selective laser melted meta-biomaterials,” *Journal of the Mechanical Behavior of Biomedical Materials,* vol. 43, pp. 91-100, 2015.

[26] S. Yavari, R. Wauthlé, J. van der Stok, A. Riemslag, M. Janssen, M. Mulier, J. Kruth, J. Schrooten, H. Weinans and A. Zadpoor, “Fatigue behavior of porous biomaterials manufactured using selective laser melting.,” *Materials Science and Engineering: C,* vol. 33, no. 8, pp. 4849-4858, 2013.

[27] “nTopology Help Centre,” nTopology, March 2021. [Online]. Available: https://support.ntopology.com/hc/en-us.

[28] *ISO 13314:2011 Mechanical testing of metals - Ductility testing - Compression test for porous and cellular metals,* ISO International.

[29] *Carpenter Additive: TECHNICAL DATA SHEET CT PowderRange Ti64 S.*

[30] S. O'Halloran, A. Connaire, A. Harte and S. Leen, “Modelling of fretting in the pressure armour layer of flexible marine risers,” *Tribology International,* vol. 100, pp. 306-316, 2016.

[31] A. Cruzado, S. Leen, M. Urchegui and X. Gómez, “Finite element simulation of fretting wear and fatigue in thin steel wires,” *International Journal of Fatigue,* vol. 55, pp. 7-21, 2013.

[32] M. Brown and K. Miller, “Theory for Fatigue Failure under Multiaxial Stress-Strain Conditions,” *Proceedings of the Institution of Mechanical Engineers,* vol. 187, no. 1, pp. 745-755, 1973.

[33] D. G. Shang, G. Q. Sun, J. Deng and C. L. Yan, “Multiaxial Fatigue Damage Models,” *Key Engineering Materials,* pp. 747-750.